(Received 24 October 2025, Accepted 24 November 2025, Scheduled 21 December 2025)

High-Sensitive Mid-Infrared Photonic Crystal Sensor Based on Slotted-Waveguide Coupled-Cavity for Acetylene Detection

Mouad Mezhoud[1,*], Hadjira Tayoub[1,2], Ahlam Harhouz[1], Farida Kebaili[1], and Abdesselam Hocini[1]

[1] *Laboratoire d'Analyse des Signaux et Systèmes, Department of Electronics, University of M'Sila BP.166, Route Ichebilia 28000, M'Sila, Algeria*
[2] *Research Center in Industrial Technologies CRTI, P. O. BOX: 64, Cheraga 16014, Algiers, Algeria*

ABSTRACT: The environment is crucial to maintaining a healthy lifestyle and ensuring the continued existence of life on Earth. Nonetheless, throughout the past several years, environmental pollution has increased significantly due to the rapid growth of the global population and technological advancement. Consequently, numerous new sensors and techniques have been developed to effectively detect different types of environmental pollutants. Among all the various methods proposed for environmental monitoring, photonic crystal (PhC) devices have demonstrated great potential in sensing applications due to their high sensitivity to refractive index change, visual detectability, room-temperature operability, and easy portability. Recently, integrated mid-infrared (mid-IR) photonics have gained considerable attention due to the fact that most gases exhibit a characteristic absorption peak in the mid-IR range. As a result, Mid-IR photonic crystals offer enormous potential for novel applications in optical interconnects and sensing. In this work, we propose a novel highly-sensitive mid-infrared photonic crystal-based slotted-waveguide coupled-cavity sensor to behave as a refractive index sensing device at a mid-infrared wavelength of 3.9 µm. The proposed sensor is simulated using Plane Wave Expansion (PWE) method and Finite-Difference Time-Domain (FDTD) algorithm. The high performance and simple design of the proposed sensor make it a promising candidate for environmental monitoring applications.

1. INTRODUCTION

Optical nano-sensors are miniature devices designed to detect and measure environmental factors at the nanoscale [1–3]. These sensors employ light and nanotechnology to monitor parameters such as pollution levels, chemical compositions, and biological contaminants in the environment. Their compact size and high sensitivity enable precise, real-time monitoring, providing valuable insights into environmental conditions [4, 5]. Optical nanosensors hold great potential for revolutionizing environmental monitoring, contributing to the protection and preservation of ecosystems worldwide.

Photonic crystal sensors offer high sensitivity and rapid response, making them highly suitable for environmental applications [5–7]. These sensors can detect minute changes in environmental parameters such as air quality [8], water quality [9–11], pollutant concentrations [5, 7, 12], and greenhouse gas levels [13]. Their compact design and potential for remote operation make them ideal for establishing efficient monitoring networks that provide real-time data essential for environmental management and informed decision-making. With their advanced capabilities, photonic crystal sensors are poised to revolutionize the way we monitor and protect the environment.

Two-dimensional photonic band gaps (PBGs) refer to wavelength ranges in which electromagnetic waves, particularly light, are prohibited from propagating in specific directions within a two-dimensional periodic structure [14, 15]. These structures, typically composed of materials with alternating high and low refractive indices arranged in a lattice pattern, forming band gaps through the constructive and destructive interference of light waves. PBGs play a vital role in photonic crystal devices by controlling light propagation, thus enabling precise manipulation of photons for applications such as optical communication [16, 17], sensing [14, 18, 19], and integrated photonics.

This work falls within this perspective, introducing a new approach for the design and analysis of refraction index (RI) sensors based on two-dimensional photonic crystals (2D-PhCs) operating in the mid-infrared region. The proposed structures are primarily based on a slotted waveguide-cavity coupling configuration. The main objective is to enhance light confinement within the cavity to improve the sensor's performance. In this study, an ultra-compact 2D-PhC mid-infrared photonic crystal sensor using slotted-waveguide coupled-cavity design is developed for environmental monitoring. The proposed sensor demonstrates promising sensing characteristics, including high sensitivity, quality factor (Q-factor), figure of merit (FOM), low detection limit, precise resonant wavelength, and strong normalized transmission. The behavior of the designed sensor is analyzed using the 2D-finite-difference time-domain (2D-FDTD) method from the RSoft software package. The high performance and simple design of the proposed sensor make it a suitable candidate for environmental monitoring.

* Corresponding author: Mouad Mezhoud (mouad.mezhoud@univ-msila.dz).

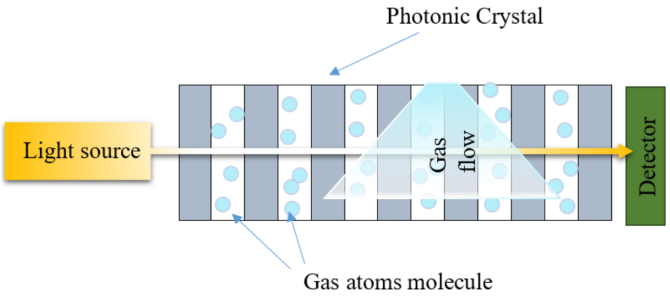

FIGURE 1. Schematic representation of a typical gas detection system based on photonic crystal structures.

2. MECHANISM OF TOXIC GAS DETECTION IN PHOTONIC CRYSTAL-BASED SENSORS

Figure 1 illustrates the schematic representation of a typical gas detection system. Photonic crystal (PhC) sensors exploit light-matter interactions to detect target gas molecules with high precision. When gas molecules are adsorbed onto the surface or infiltrate in the holes of the PhC structure, they induce a change in the local refractive index of the sensing region. This refractive index variation modifies the photonic band structure, leading to measurable shifts in the transmission or reflection spectra. By analysing these spectral shifts, the presence, type, and concentration of the target gas can be occurately identified.

The specific mechanism of gas detection depends on the design and structure of the photonic crystal. For instance, some photonic crystal sensors employ a resonant cavity design, in which the adsorption of gas molecules causes a shift in the cavity's resonant wavelength. Other designs may exploit changes in the material's photonic bandgap, which can be monitored using spectroscopic techniques.

3. MATHEMATICAL BACKGROUND AND PROPOSED DESIGN

3.1. Mathematical Background

In this work, the Plane Wave Expansion (PWE) method is employed to model the photonic crystal and determine the photonic band gaps for both TE and TM modes. The Finite-Difference Time-Domain (FDTD) method is used to solve Maxwell's equations through the RSoft software. The proposed sensor is discretized using fine computational grids (Δx, Δy) with grid sizes optimized through multiple FDTD simulations. Since the boundary conditions at the spatial boundaries of the computational domain are critical, a perfectly matched layer (PML) of one spatial unit thickness surrounds the simulation area to absorb outgoing fields and minimize reflections [20, 21]. The propagation of light in a PhC sensor is obtained by solving Maxwell's electromagnetic equations as follows [22]:

$$\nabla \times \left(\frac{1}{\varepsilon}\nabla \times H\right) = \left(\frac{\omega}{c}\right)^2 H \tag{1}$$

where ε is the permittivity; H is the magnetic field; ω is the angular frequency; C is the speed of light.

In this work, to ensure a stable simulation, one must adhere to the courant condition which relates the spatial and temporal step size [23, 24]:

$$C\Delta t < \frac{1}{\sqrt{(1/\Delta x^2 + 1/\Delta y^2 + 1/\Delta z^2)}} \tag{2}$$

In the band structure computation of a PhC, the dispersion relation is calculated by PWE method. This requires solving the eigenvalue problem derived from the Helmholtz equation for an infinite periodic structure. The resulting dispersion relation is expressed as follows [25]:

$$\hat{\theta}H = \left(\frac{\omega^2}{c^2}\right) H \tag{3}$$

where:

$$\hat{\theta} = -\left(\frac{\partial}{\partial x}\right)\left(\frac{1}{\epsilon(x)}\right)\left(\frac{\partial}{\partial x}\right) \tag{4}$$

x is the periodic dielectric function.

The optical refractive index (RI) of a medium is a key parameter in describing light-matter interactions. In this work, we evaluate the overall performance of the sensor using two important metrics: Sensitivity (S) and Figure of merit (FoM).

These are calculated as follows [26]:

$$S = \frac{\Delta\lambda_0}{\Delta n_{analyte}} = \frac{\Delta\lambda_0}{\Delta n}\left(\frac{nm}{RIU}\right) \tag{5}$$

$$FoM = \frac{S}{(FWHM)}\left(RIU^{-1}\right) \tag{6}$$

where $\Delta\lambda_0$ is the shift in the resonant wavelength; Δn is the change in the refractive index; and FWHM is the full width at half maximum.

The Figure of Merit (FoM) is also proportional to the quality factor (Q), which is defined as follows:

$$Q = \frac{\lambda_0}{FWHM} \tag{7}$$

3.2. The Basic Structure of the Proposed Gas Sensor

The 2D-PhC device consists of air holes ($n_{air} = 1$) etched into a silicon membrane with a refraction index of $n_{Si} = 3.42$. The structure contains 22×23 holes along the X and Z directions. The distance between the centers of two adjacent holes, known as the lattice constant or periodicity (a), is 1.1 µm. The radius of each hole is defined as $r = a \times 0.29$ µm.

Using the Plane Wave Expansion (PWE) method, the photonic band diagram of the host structure was calculated. The results show the presence two normalized band gaps in the TM polarization mode, as summarized in Table 1.

Figure 2 shows the photonic band structure of the 2D photonic crystal for both transverse electric (TE) and transverse magnetic (TM) polarizations along the high-symmetry path Γ-M-K-Γ. A well-defined TM bandgap is observed between normalized frequencies 0.20–0.26, whereas a partial TE bandgap

TABLE 1. Photonic band gaps (PBGs) of the proposed 2D-PhC structure for TM polarization.

Photonic band gap (PBGs)		Frequency range	Wavelength range (μm)
TM	Band 1	$0.58483 \leq (f = a/\lambda) \leq 0.61453$	$1.78998 \leq \lambda \leq 1.88088$
	Band 2	$0.20736 \leq (f = a/\lambda) \leq 0.2681$	$4.1029 \leq \lambda \leq 5.30478$

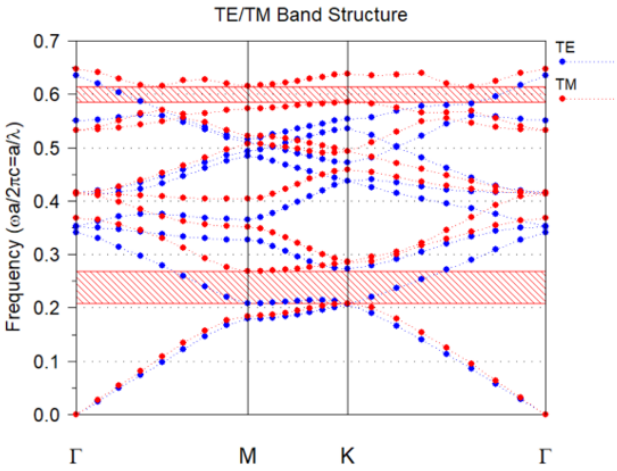

FIGURE 2. Band structure diagram of the connected photonic crystal structure.

appears around 0.58–0.61. These results indicate that the structure can effectively confine and guide light at the corresponding frequencies. The presence of a distinct TM bandgap is crucial for sensor performance, as it enables strong field localization within the designed nanocavities, which in turn leads to enhanced sensitivity to refractive index changes.

3.3. Gas Sensor Based on a Guide-Cavity Coupling

The schematic representation of the first proposed structure is shown in Figure 3, the waveguide is formed by removing a single row of air holes along the ΓK direction of the triangular lattice. The initial lattice parameters consist of a triangular array of air holes with periodicity (a) and hole radius (r). The Gaussian source is placed at the input end of the waveguide (W1), while a monitor is positioned at its output to record the transmission spectrum. The proposed cavity is created by inserting an air slot and six additional air holes at the center of the waveguide. The slot width (Z-Slot) and slot length (X-Slot) define the cavity dimensions and are optimized to achieve maximum light confinement and sensitivity.

4. RESULTS AND DISCUSSIONS

4.1. Study of the Proposed Sensor

To develop a miniaturized photonic crystal toxic gas sensor with high sensitivity and FoM, a resonance-based design is proposed. The proposed sensor consists of a coupled waveguide integrated with a slot resonator incorporating three holes on each side of the cavity. The geometric parameters of the proposed structure are as follows: X-slot = 460 nm, Z-slot = 30 nm, $r = 0.29 \times a$ and $n_{\text{air}} = 1$, and $n_{\text{subsrate}} = 3.42$.

The numbers of holes on both sides, as well as the values of X-slot and Z-slot, were chosen to ensure effective coupling among the central resonator, the input waveguide, and the output waveguide.

In this section, the numerical simulations corresponding to the interaction of incident waves with the designed sensor are presented. To investigate the effect of the slot coupled with the waveguide, the transmission spectra were numerically calculated using the 2D Finite-Difference Time-Domain (2D-FDTD) method, as shown in Figure 5. Multiple resonance modes can be generated based on this design. When the slot resonator is inserted into the waveguide, destructive interference occurs between the guided mode (supported by the waveguide) and the resonant modes (created by the central slot) resulting in two sharp resonance peaks in the transmission spectrum at ($\lambda_{\text{M1res}} = 5.220291$ μm, $\lambda_{\text{M2res}} = 5.336174$ μm).

As shown in Figure 4(a), the transmission peaks (T_{peak}) reach 95% and 87% for the two resonance modes, respectively. The transmission spectrum presented in Figure 4(a), exhibits resonance line shapes with sharp and well-defined profiles. Near the resonance wavelengths, the transmission transitions rapidly between 0% and 95 %, indicating that constructive and destructive interferences occur in cproximity. This behavior arises from the rapid phase variation along the localized (resonance-assisted) pathway compared to the background pathway. The quality factor (Q) of the two resonance modes are 3.8×10^6 and 1.58×10^6, respectively. The corresponding full width at half maximum (FWHM) values at −3 dB are 0.00309 μm for the first mode and 0.00367 μm for the second mode.

To better understand the proposed sensor behavior, Figures 4(b)–(d) illustrate the magnetic field distribution ($|Hy|$) of the proposed sensor at the resonance wavelengths $\lambda_0 = 5.220291$ μm and 5.336174 μm. It is evident that the magnetic field is strongly confined within the slot resonator. Based on this observation, the effect of varying the geometric parameters of the slot was further investigated to optimize the sensor's detection performance

The resonance peaks are highly sensitive to changes in the refractive index near the region of magnetic field confinement ($|Hy|$). By varying the refractive index of the air holes from $n = 1$ to $n = 1.002$, a measurable shift in the resonance spectrum is induced. The corresponding sensitivity calculated for $\Delta n = 0.002$ is 545.5 nm/RUI for the first mode and 285 nm/RUI for the second mode.

4.2. Effect of Slot Geometric Parameters

The performance of the proposed photonic crystal sensor is strongly influenced by the geometric parameters of the slot resonator including its length (X-Slot) and width (Z-Slot). In this section, the slot width Z-Slot was fixed at 0.3 μm while the slot

TABLE 2. Variation of FWHM, quality factor (Q), and figure of merit (FoM) as a function of the X-Slot variation.

X-Slot (μm)	FWHM (μm)		Q		FoM	
	M1	M2	M1	M2	M1	M2
4.2	0.00262	0.00386	1.2×10^7	1.58×10^6	6.31×10^5	8.51×10^4
4.4	0.00203	0.0025	5.65×10^6	1.51×10^6	5.91×10^5	8.08×10^4
4.6	0.00309	0.00367	3.81×10^6	1.58×10^6	3.98×10^5	8.46×10^4
4.8	0.00289	0.00302	1.90×10^6	2.87×10^6	1.98×10^5	1.53×10^5

TABLE 3. Variation of FWHM, quality factor, and FoM as a function of the change in Z-Slot.

Z-Slot (μm)	FWHM (μm)		Q		FoM	
	M1	M2	M1	M2	M1	M2
0.9	4.3709×10^{-4}	0.00339	1.07×10^7	1.4×10^6	1.51×10^6	2.23×10^5
0.8	9.2571×10^{-4}	0.00354	5.17×10^6	1.45×10^6	7.42×10^5	2.23×10^5
0.7	0.00137	0.00337	3.52×10^6	1.53×10^6	6.78×10^5	2.38×10^5
0.6	0.00275	0.00186	1.80×10^6	2.86×10^6	2.68×10^5	3.03×10^5

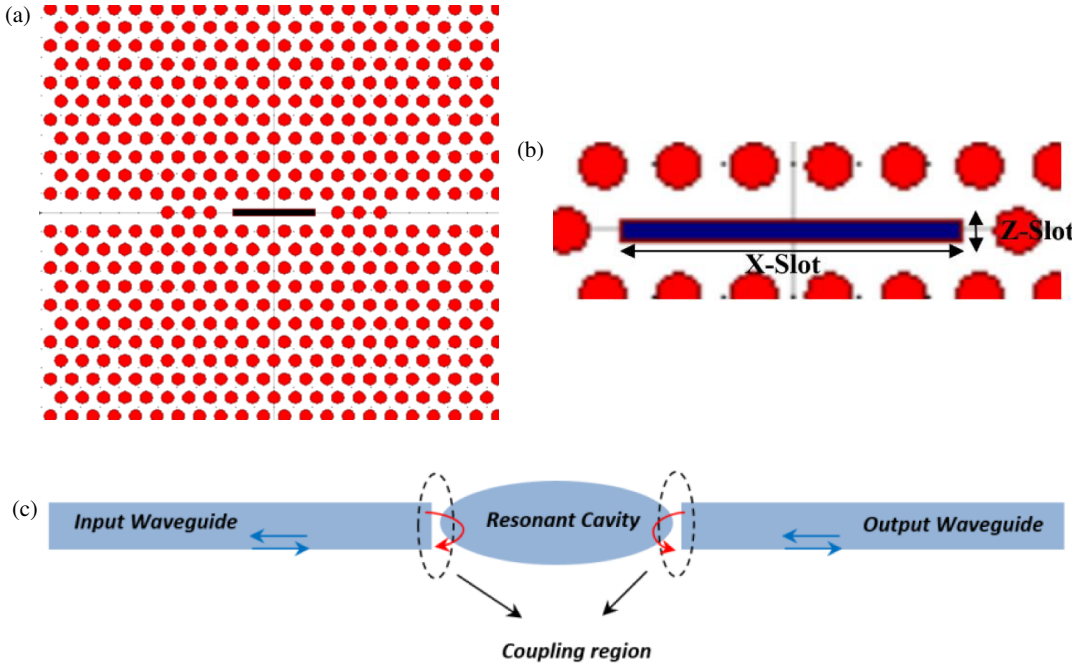

FIGURE 3. (a) The proposed design of the toxic gas sensor. (b) Schematic illustration of the geometric parameters of the central cavity. (c) Coupled-cavity configuration illustrating the realization of the resonant effect.

length (X-Slot) was varied from 4.2 μm to 4.8 μm in steps of 0.02. The shifts of the resonant modes, as well as the transmission and sensitivity of the sensor, were simulated for the different X-Slot values and are presented in Figure 5. It is very clear that the highest transmission and sensitivity are achieved for X-Slot $= 4.4$ μm.

Table 2 presents the variation of the FWHM, quality factor (Q), and figure of merit (FoM) as a function of X-Slot. It is evident that for both modes, the FWHM values are low, which is highly desirable for accurate measuring of refractive index variations. The quality factor (Q) ranges between 1.51×10^6 and 1.2×10^7.

In the next step, the same scenario was applied with the slot length (X-Slot) fixed at 4.4 μm, while the slot width (Z-Slot) was varied from 0.6 μm to 0.9 μm in increments of 0.05.

The sensitivity of the proposed sensor for the different Z-Slot values was simulated and is shown in Figure 6. The results clearly indicate that the highest sensitivity is achieved for Z-Slot $= 0.7$ μm.

Table 3 summarizes the corresponding variations of FWHM, quality factor (Q), and FoM as a function of Z-Slot. As with the

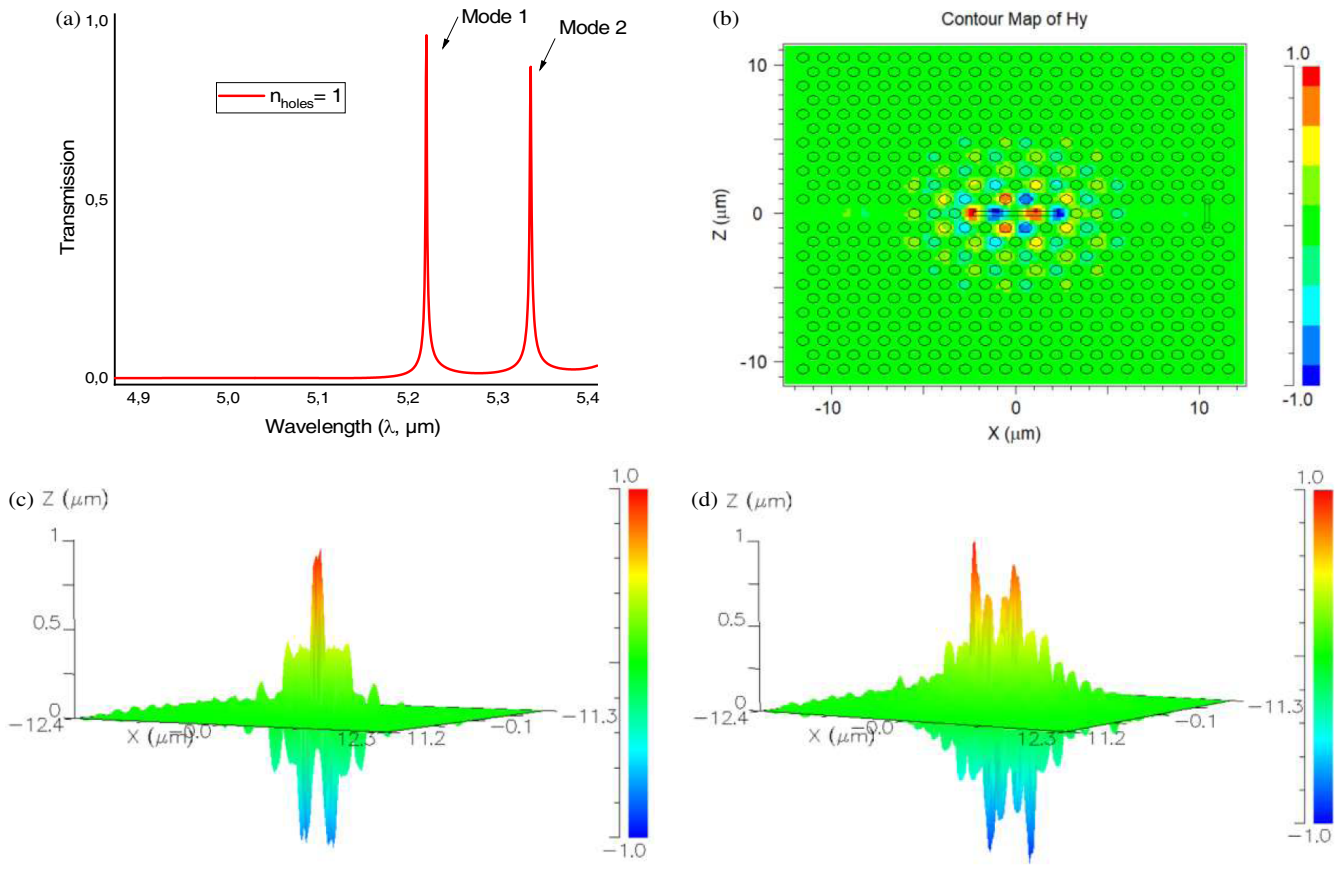

FIGURE 4. (a) Transmission spectrum of the coupled system, (b) Two-dimensional (2D) distribution of magnetic field intensity ($|H|$ for the second resonant mode. (c) (d) Three-dimensional (3D) distributions of magnetic field intensity ($|H|$ at the two resonant wavelengths (Mode 1 and Mode 2).

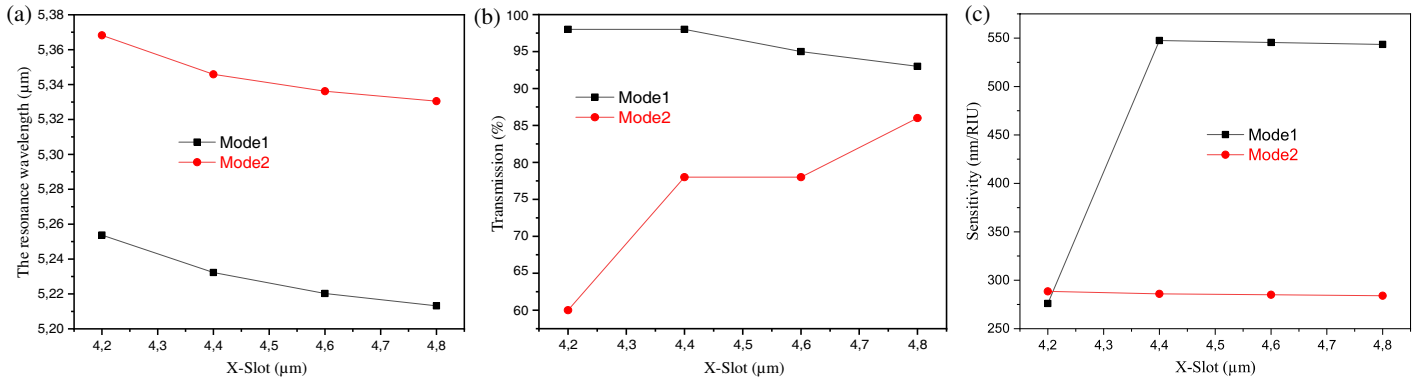

FIGURE 5. Variation of (a) the resonant wavelength, (b) the transmission, and (c) the sensitivity as a function of the X-Slot variation.

X-Slot analysis, the FWHM values remain low for both modes, confirming excellent resolution for refractive index detection. The quality factor (Q) varies between 1.48×10^6 and 1.07×10^7.

4.3. Optimized Sensor

As mentioned, the resonant modes are highly sensitive to variation in the refractive index around the region of the magnetic field distribution ($|Hy|$). To further enhance the transmission and the sensitivity of the proposed sensor, an air hole with radius R_C is introduced at the center of the slot resonator (Figure 7). The presence of this central hole improves light confinement and strength the field-matter interaction within the sensing region, thereby optimizing the performance of the proposed sensor (Figure 8).

4.4. Application of the Proposed PhC Sensor for Acetylene Gas Monitoring

Acetylene (C_2H_2) is an organic gas that contributes to the formation of photochemical oxidants and to global warming. It is therefore classified as a Volatile Organic Compound (VOC),

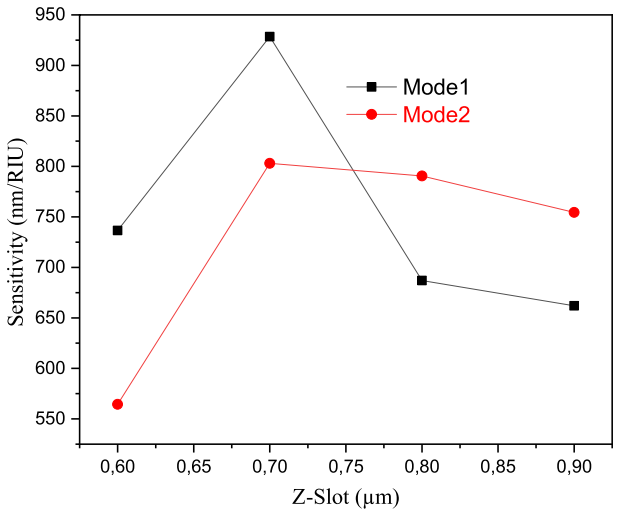

FIGURE 6. Variation of the (a) resonant wavelength, (b) transmission, and (c) sensitivity as a function of the change in Z-Slot.

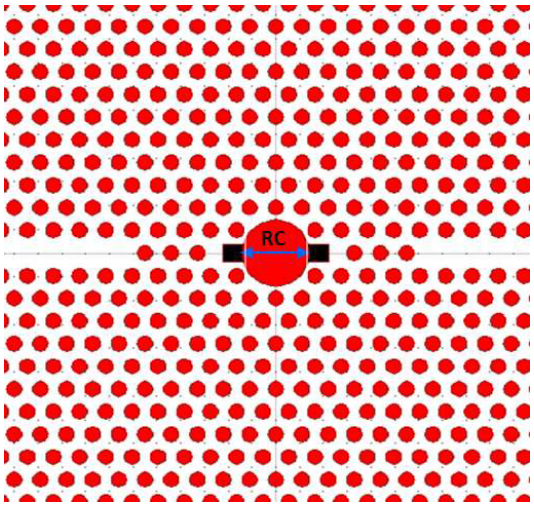

FIGURE 7. Schematic representation of the optimized PhC sensor.

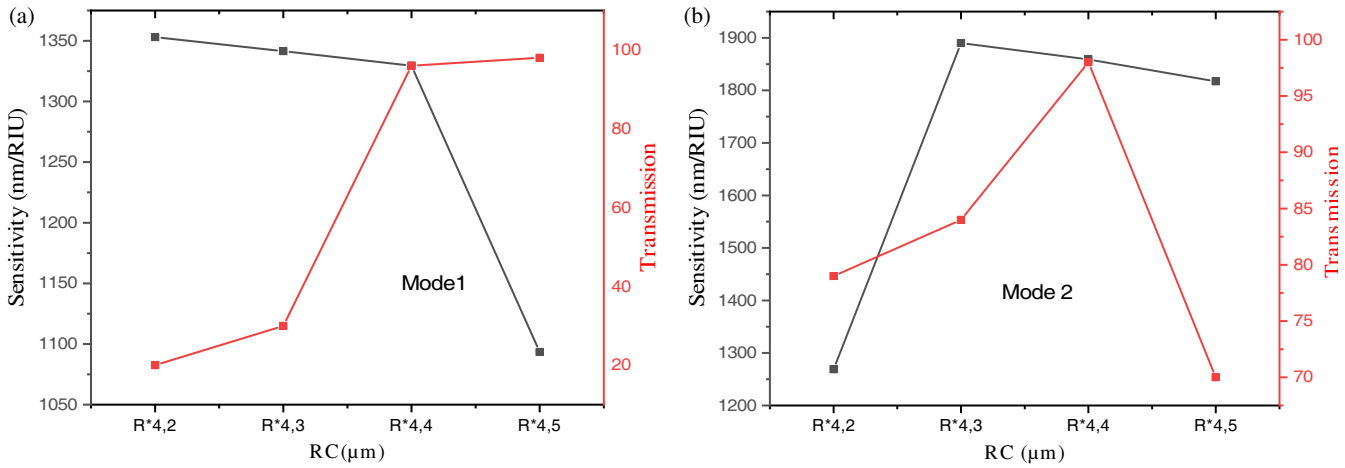

FIGURE 8. Variation of the transmission and sensitivity as a function of the change in the central air hole radius (R_C), (a) Mode 1 and (b) Mode 2.

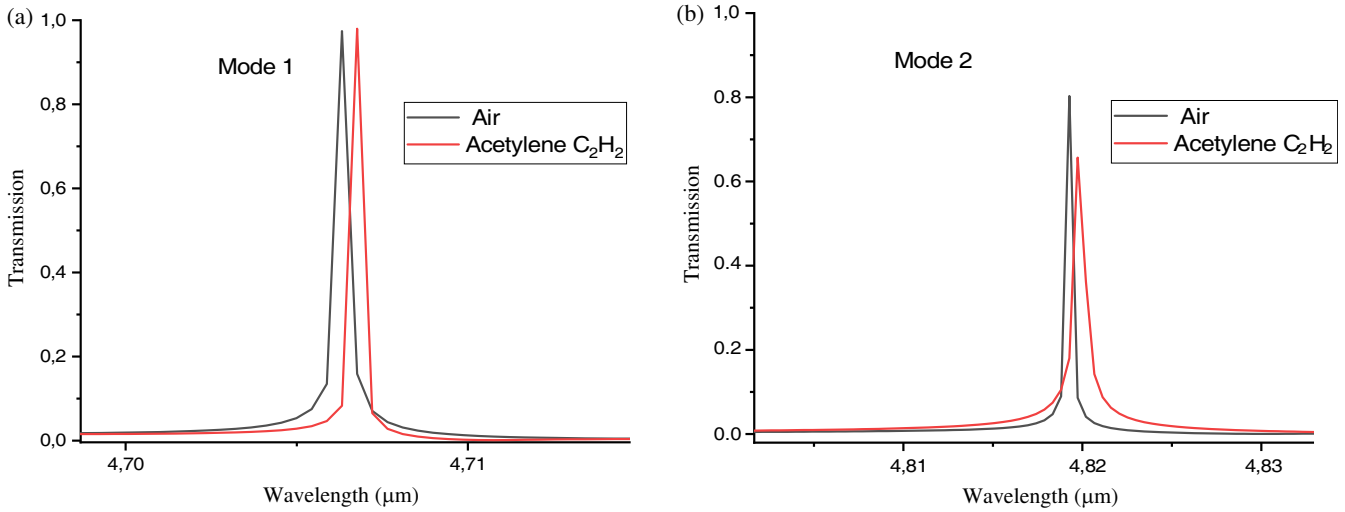

FIGURE 9. Transmission spectrum of the optimized for the acetylene gas sensor, (a) Mode 1 and (b) Mode 2.

and specific legal requirements for VOC emissions reporting may vary depending on the national regulations

Chemically represented as C_2H_2 ($n = 1.000579$) [27], acetylene is a colorless and highly flammable gas with a distinct garlic-like odor. It is typically produced by the reaction between calcium carbide and water. Due to its high flame temperature-reaching up to 3500°C (6330°F) in oxygen-rich environments, acetylene is widely used in oxy-fuel welding and cutting applications. It also serves in organic synthesis and a precursor in the production of plastics and chemicals. However, its highly explosive nature necessitates careful handling, storage, and transportation.

In this study, it is assumed that the air holes ($n = 1000265$) in the proposed structure are completely infiltrated with acetylene (C_2H_2, $n = 1000579$). Figure 9 illustrates the transmission spectrum of the structure obtained using the 2D-FDTD method. A resonant wavelength shift of 0443 nm is observed for the first mode, corresponding to a sensitivity of 14108 nm/RIU. Similarly, a shift of 0.465 nm is obtained for the second mode, resulting in a sensitivity of 148089 nm/RIU. These results confirm the high sensitivity and strong detection capability of the proposed PhC sensor for acetylene gas monitoring.

Table 4 presents a brief comparison between the proposed biosensor and other reported biosensors to demonstrate the validity and effectiveness of the proposed design. All the listed structures are based on two-dimensional photonic crystal waveguides coupled with resonator cavities of various geometries. All the structures listed are based on 2D photonic crystals waveguides coupled with resonator cavities of various geometries.

TABLE 4. Comparison between the literatures and the proposed sensor.

References	Sensitivity (nm/RIU)	Q-actor	Year
[28]	650	*	2019
[7]	1343.2	*	2021
Our proposed biosensor	1480.89	10^7	—

As shown in the table, our proposed biosensor showed remarkably higher sensitivity, high Q-factor.

5. CONCLUSION

In this work, a PhC-based sensor for gas detection has been proposed, utilizing the refractive index (RI) variation principle. The designed device consists of a waveguide coupled with a slot resonator. FDTD simulation results demonstrate that even small changes in the RI of the infiltrated gas lead to a noticeable shift in the resonance wavelength, indicating high sensitivity. The optimized sensor exhibits excellent performance with high sensitivity, quality factor (Q), and figure of merit (FoM), making it competitive with existing state-of-art PhC gas sensors.

REFERENCES

[1] Naik, R., A. N. Kumar, H. P. Nagaswarupa, and S. G. Reddy, "Optical nanotechnology-based sensors for environmental contaminants' detection," in *Nanotechnology-based Sensors for Detection of Environmental Pollution*, 137–153, Elsevier, 2024.

[2] Abdel-Karim, R., "Advanced approaches in micro-and nanosensors for harsh environmental applications: A review," in *Modern Nanotechnology: Volume 1: Environmental Sustainability and Remediation*, 585–612, Springer, 2023.

[3] Wang, F., Z. Meng, F. Xue, M. Xue, W. Lu, W. Chen, Q. Wang, and Y. Wang, "Responsive photonic crystal for the sensing of environmental pollutants," *Trends in Environmental Analytical Chemistry*, Vol. 3-4, No. 2014, 1–6, 2014.

[4] Scullion, M. G., T. F. Krauss, and A. D. Falco, "Slotted photonic crystal sensors," *Sensors*, Vol. 13, No. 3, 3675–3710, 2013.

[5] Mou, F. A., M. M. Rahman, M. R. Islam, and M. I. H. Bhuiyan, "Development of a photonic crystal fiber for wave guidance and environmental pollutants detection," *Sensing and Bio-Sensing Research*, Vol. 29, 100346, 2020.

[6] De, M., T. K. Gangopadhyay, and V. K. Singh, "Prospects of photonic crystal fiber as physical sensor: An overview," *Sensors*, Vol. 19, No. 3, 464, 2019.

[7] Tayoub, H., A. Hocini, and A. Harhouz, "High-sensitive mid-infrared photonic crystal sensor using slotted-waveguide coupled-cavity," *Progress In Electromagnetics Research M*, Vol. 105, 45–54, 2021.

[8] Bouzidi, A., D. Bria, A. Akjouj, Y. Pennec, and B. Djafari-Rouhani, "A tiny gas-sensor system based on 1D photonic crystal," *Journal of Physics D: Applied Physics*, Vol. 48, No. 49, 495102, 2015.

[9] Harhouz, A. and A. Hocini, "Design of high sensitive optical sensor for seawater salinity," in *2nd International Congress on Energy Efficiency and Energy Related Materials (ENEFM2014)*, 219–225, 2015.

[10] Shi, Q., J. Zhao, and L. Liang, "Two dimensional photonic crystal slab biosensors using label free refractometric sensing schemes: A review," *Progress in Quantum Electronics*, Vol. 77, 100298, 2021.

[11] Arunbabu, D., A. Sannigrahi, and T. Jana, "Photonic crystal hydrogel material for the sensing of toxic mercury ions (Hg 2+) in water," *Soft Matter*, Vol. 7, No. 6, 2592–2599, 2011.

[12] Kou, D., Y. Zhang, S. Zhang, S. Wu, and W. Ma, "High-sensitive and stable photonic crystal sensors for visual detection and discrimination of volatile aromatic hydrocarbon vapors," *Chemical Engineering Journal*, Vol. 375, 121987, 2019.

[13] Ahmed, F., V. Ahsani, K. Nazeri, E. Marzband, C. Bradley, E. Toyserkani, and M. B. G. Jun, "Monitoring of carbon dioxide using hollow-core photonic crystal fiber mach-zehnder interferometer," *Sensors*, Vol. 19, No. 15, 3357, 2019.

[14] Hocini, A. and A. Harhouz, "Modeling and analysis of the temperature sensitivity in two-dimensional photonic crystal microcavity," *Journal of Nanophotonics*, Vol. 10, No. 1, 016007, 2016.

[15] Tayoub, H., A. Harhouz, and A. Hocini, "2D photonic crystal biosensing platform based on coupled defective ring-shaped microcavity-two waveguides for diabetes detection using human tears," *Physica Scripta*, Vol. 98, No. 11, 115510, 2023.

[16] Benisty, H., C. Weisbuch, D. Labilloy, M. Rattier, C. J. M. Smith, T. F. Krauss, R. M. D. L. Rue, R. Houdre, U. Oesterle, C. Jouanin, and D. Cassagne, "Optical and confinement properties of two-dimensional photonic crystals," *Journal of Lightwave Technology*, Vol. 17, No. 11, 2063–2077, 1999.

[17] Parandin, F., R. Kamarian, and M. Jomour, "Optical 1-bit comparator based on two-dimensional photonic crystals," *Applied Optics*, Vol. 60, No. 8, 2275–2280, 2021.

[18] Zouache, T., A. Hocini, A. Harhouz, and R. Mokhtari, "Design of pressure sensor based on two-dimensional photonic crystal,"

Acta Physica Polonica A, Vol. 131, No. 1, 68–70, 2017.

[19] Parandin, F., F. Heidari, Z. Rahimi, and S. Olyaee, "Two-dimensional photonic crystal biosensors: A review," *Optics & Laser Technology*, Vol. 144, 107397, 2021.

[20] Harhouz, A. and A. Hocini, "Design of high-sensitive biosensor based on cavity-waveguides coupling in 2D photonic crystal," *Journal of Electromagnetic Waves and Applications*, Vol. 29, No. 5, 659–667, 2015.

[21] Hocini, A., R. Moukhtari, D. Khedrouche, A. Kahlouche, and M. Zamani, "Magneto-photonic crystal microcavities based on magnetic nanoparticles embedded in silica matrix," *Optics Communications*, Vol. 384, 111–117, 2017.

[22] Yee, K., "Numerical solution of initial boundary value problems involving Maxwell's equations in isotropic media," *IEEE Transactions on Antennas and Propagation*, Vol. 14, No. 3, 302–307, 1966.

[23] Taflove, A. and M. E. Brodwin, "Numerical solution of steady-state electromagnetic scattering problems using the time-dependent Maxwell's equations," *IEEE Transactions on Microwave Theory and Techniques*, Vol. 23, No. 8, 623–630, 1975.

[24] Kunz, K. S. and R. J. Luebbers, *The Finite Difference Time Domain Method for Electromagnetics*, CRC Press, 1993.

[25] Chhoker, P. and S. Bajaj, "Analysis of photonic band structure in 1-D photonic crystal using PWE and FDTD Method," *IJISET — International Journal of Innovative Science, Engineering & Technology*, Vol. 2, No. 8, 883–887, 2015.

[26] Hajshahvaladi, L., H. Kaatuzian, and M. Danaie, "Design of a hybrid photonic-plasmonic crystal refractive index sensor for highly sensitive and high-resolution sensing applications," *Physics Letters A*, Vol. 420, 127754, 2021.

[27] Troia, B., A. Paolicelli, F. D. Leonardis, and V. M. N. Passaro, *Photonic Crystals for Optical Sensing: A Review*, Advances in Photonic Crystals, 2013.

[28] Tayoub, H., A. Hocini, and A. Harhouz, "Mid-infrared refractive index sensor based on a 2D photonic crystal coupled cavity-two waveguides," *Instrumentation, Mesures, Métrologies*, Vol. 18, No. 2, 165–169, 2019.